Journal of Catalysis **194,** 167–174 (2000)
doi:10.1006/jcat.2000.2921, available online at http://www.idealibrary.com on IDEAL®

Fe/MgO Formulations for the Catalytic Combustion of Methane

R. Spretz,* S. G. Marchetti,† M. A. Ulla,* and E. A. Lombardo*,[1]

*Instituto de Investigaciones en Catálisis y Petroquímica, INCAPE (FIQ, UNL-CONICET), Santiago del Estero 2829, C.P. 3000, Santa Fe, Argentina; and †Centro de Investigación y Desarrollo en Procesos Catalíticos, CINDECA (UNLP-CONICET), Calle 47 No. 257, C.P. 1900, La Plata, Argentina

Received October 25, 1999; revised May 5, 2000; accepted May 5, 2000

Fe/MgO catalysts containing between 1.5 and 9 wt% iron were prepared by impregnation and calcined at 1073 K for 10 h. The solids were characterized by XRD and Raman and Mössbauer spectroscopies. They all showed that the solids are made up of $MgFe_2O_4$ spinel clusters and Fe^{3+} dispersed in the MgO matrix. The concentrations of $MgFe_2O_4$ and Fe^{3+} were calculated from the Mössbauer data. The former increases by a factor of 23 while the latter remains almost constant when the iron loading varies between 1.5 and 9 wt%. The catalytic activity correlates with the spinel weight fraction in the Fe/MgO system. Both the SEM micrographs and the EPMA analyses of the catalysts indicate that the solid surface is made up of exposed patches of $MgFe_2O_4$ and MgO. This surface feature explains the plateau observed when the reaction rate constant is plotted versus the iron loading.

Key Words: **methane combustion; Fe/MgO; $MgFe_2O_4$; CH_4 oxidation.**

INTRODUCTION

Since Pfefferle and Pfefferle (1) proposed catalytic combustion as an efficient method for burning fuels in an environmentally friendly way, considerable progress has been made in materials development and engineering design. However, a number of issues concerning high-temperature applications are still far from being solved, despite the fact that the first commerical unit installed in an electrical utility has recently begun to operate (2). There is also little information on the kinetics, mechanism, and nature of the active sites involved in this reaction.

The preferred approach in catalytic combustion applications is the use of hybrid systems (3). The separation of the combustion process into two well-defined zones allows a better control of the whole system. In the high-temperature zone the catalyst should be resistant to severe hydrothermal conditions (4). Spinels of different types, among other mixed oxides, are good candidates for this application in view of their high thermal stability (5).

[1] To whom correspondence should be addressed. E-mail: nfisico@fiqus.unl.edu.ar.

Berg and Järås have already targeted MgO as a support for high-temperature catalytic combustion (6), due to its ability to maintain a larger surface area at high temperature than most other oxides employed as catalyst supports. The addition of iron to MgO may lead to the formation of a spinel phase. In fact, the Fe/MgO system, in both the reduced and oxidized forms, has already been used as catalyst. Reduced, it has been used for ammonia synthesis. Boudart *et al.* (7–9), who employed Mössbauer spectroscopy to characterize this system in the reduced form, identified the presence of small metallic particles in Fe/MgO and Fe^{2+} clusters in MgO. Ueda *et al.* (10–12) studied the catalytic performance of Fe/MgO in the oxidized form in cross-coupling reactions leading to the production of α,β-unsaturated compounds. Asakura and Iwasawa (13) characterized this system using EXAFS and XANES. They concluded that there exist small cluster structures of $MgFe_2O_4$ in the MgO lattice. Based on their XANES data, they also said that Fe^{3+} cations are present at the interface between $MgFe_2O_4$ and the parent MgO lattice.

In this work, we report data concerning the catalytic performance of Fe/MgO for the combustion of methane. Furthermore, in order to give insights into the nature of the active sites, we also report data obtained using several characterization techniques.

EXPERIMENTAL

Catalyst Preparation

The catalysts were prepared by impregnation. A 0.5 M $Fe(NO_3)_3 \cdot 9H_2O$ (Merck, p.a.) solution was added to an MgO (Alfa, p.a.) suspension in distilled water. This suspension was prepared by adding ca. 100 ml per 5 g of solid. The amount of the $Fe(NO_3)_3$ solution used was that necessary to obtain the desired Fe content. After the addition of the ferric solution to the suspension, the pH value was ca. 10, where the immediate precipitation of the hydroxide took place. The solids prepared contained 1.5, 3, 6, and 9 wt% Fe, which hereafter will be referred to as Fe(w)/MgO, where w is the weight percentage. The resulting slurry was intensely

0021-9517/00 $35.00

stirred on a hot plate until dryness was achieved. The solid so obtained was kept in an oven at 383 K overnight. Finally, it was calcined in air flow at 1073 K for 10 h. An aliquot of the support was also calcined under the same conditions.

The model solids, α-Fe_2O_3 and the $MgFe_2O_4$ spinel, were synthesized. For the preparation of α-Fe_2O_3, concentrated ammonia was added to a 0.5 M $Fe(NO_3)_3 \cdot 9H_2O$ solution in order to precipitate the Fe^{3+} in the hydroxide form. The solid was filtered under vacuum and the cake obtained was washed several times with distilled water. The hydroxide was then dried in an oven and finally calcined at 1223 K in air flow for 5 h. The spinel was prepared by mixing $Mg(CH_3COO)_2$ (Merck, p.a.) and $Fe(NO_3)_3 \cdot 9H_2O$ solutions (both 0.5 M) in stoichiometric proportion. Then, a 1 M citric acid solution was added in an amount equivalent to the total cations. The resulting solution was kept in an oven at 383 K until dryness. This precursor was calcined in air flow at 1223 K for 10 h.

Catalyst Characterization

The BET surface area of the solids was determined using a Quantachrome Nova 1000 Sorptometer. The samples were evacuated for 3 h at 573 K before measuring the surface area. In the experiments, nine relative pressure values were selected in the range of 0.05 to 0.25 Torr.

The X-ray diffraction patterns were obtained using an XD-D1 Shimadzu instrument with monochromator employing Cu$K\alpha$ radiation. The scan rate was 1° per minute. The diffractograms were acquired at a voltage of 30 kV and an intensity of 40 mA.

The Raman spectra were obtained under ambient conditions using a JASCO TRS-600SZ-P single monochromator spectrophotometer equipped with an intensified photodiode array cooled to about 150 K with liquid N_2. The excitation source was the 514.5 nm line of a Spectra 9000 Photometrics Ar ion laser. The laser power, measured at the samples, was set at 30–40 mW.

The Mössbauer spectra were acquired with a standard 512-channel spectrometer with transmission geometry. The samples were placed in an He closed-cycle refrigerator at temperatures ranging from 16 to 298 K. A ^{57}Co-in-Rh matrix source of nominally 50 mCi was used. The velocity calibration was performed against a 6-μm-thick α-Fe foil. All isomer shifts were referred to this standard at 298 K. Spectra were fitted by using a least-squares nonlinear computer-fitting program with constraints. Lorentzian lines were considered with equal widths for each spectrum component. The baseline was fitted to a second-order polynomial, and the velocity nonlinearity was fitted to a third-order polynomial. The spectra were folded to minimize geometric effects.

The morphology of different materials was studied using a Jeol microscope, JSM-35C model, operated at accelerating voltages of 20–25 kV. The samples were glued to the sample holder using silver paint. The preparations were covered with a thin gold layer to obtain better images. An electron probe microanalyzer (EPMA) was used for the chemical microanalysis of Fe(w)/MgO ($w = 3$, 6, and 9) and $MgFe_2O_4$. The X-ray beam was concentrated in a volume of about 1 μm^3. Different regions of the same particle were tested.

Catalytic Measurements

The catalytic activity of Fe(w)/MgO for methane combustion was measured using a quartz microreactor, 4 mm i.d. (6 mm o.d.) and 30 cm long, operated in plug flow mode. A 0.050 g portion of catalyst was lodged in the reactor center part between two quartz wool plugs. The catalyst particle size was 60–80 mesh. The oven surrounding the reactor was 30 cm long to ensure that the reactants reached the reaction temperature at the catalyst bed inlet. A thermocouple attached to the external side of the reactor wall was used to measure the reaction temperature.

CH_4, O_2, and N_2 were fed using mass flow controllers. To avoid excessive thermal effects and water condensation downstream of the reactor, the methane concentration was limited to 2% v/v. The oxygen concentration was 100% in excess of the stoichiometric value to ensure complete oxidation to CO_2 and H_2O. The typical hourly space velocity was 480,000 h^{-1}. To achieve steady state, the reactor was kept at each temperature for 30 min before conversion measurements. The analysis of the reacting stream was carried out using an online chromatograph equipped with a Porapak Q column and a TCD. The carbon balance was in all cases within a 5% tolerance. The conversion values reported here represent the average for three gas samples analyzed. The reaction rates were calculated using conversion data obtained by operating the reactor in differential mode. The maximum value of methane conversion achieved was 12.9%. This corresponds to runs performed with the most active catalysts at the highest reaction temperature (948 K).

RESULTS

X-Ray Diffraction and Raman Spectroscopy Data

The XRD data of the Fe(w)/MgO catalysts, with $w = 1.5$, 3, 6, and 9%, present the support reflections as shown in Table 1, in addition to three weak ones corresponding to the iron-containing phase. An increase in the intensity of the latter ones with the amount of supported Fe can be observed. The pattern of the 1.5 wt% iron sample only shows the support reflections.

By comparing the diffractograms of the Fe/MgO series with the ones corresponding to the model solids, we can conclude that the three additional signals observed in the patterns of the Fe/MgO samples belong to $MgFe_2O_4$; the

TABLE 1

Structural Characteristics of Fe/MgO Catalysts and the Model Compounds

Solid	Main XRD reflections,[a] 2θ (deg)			Raman bands (cm^{-1})		S_g[c] ($m^2 \cdot g^{-1}$)
	MgO	$MgFe_2O_4$[b]	α-Fe_2O_3	$MgFe_2O_4$	α-Fe_2O_3	
α-Fe_2O_3	—	—	33.16 (100)	—	498, 612	—
$MgFe_2O_4$	—	30.13 (35), 35.50 (100), 56.98 (31)	33.22 (6)	472, 542, 638, 714	—	0.6
Fe(1.5)/MgO	42.94 (100), 62.29 (51)	—	—	(Fluorescence only)	—	37.3
Fe(3)/MgO	42.94 (100), 62.32 (49)	30.13 (1), 35.54 (3), 57.01 (1)	—	473, 553, 643, 716	—	31.1
Fe(6)/MgO	42.94 (100), 62.35 (47)	30.13 (3), 35.47 (9), 57.07 (2)	—	477, 551, 651, 715	—	26.7
Fe(9)/MgO	42.94 (100), 62.29 (46)	30.07 (4), 35.47 (16), 57.04 (4)	—	479, 552, 652, 716	—	19.6

[a] The relative intensities are indicated in parentheses.
[b] Another intense signal of $MgFe_2O_4$ which appears at 62.54° (relative intensity, 47%) overlaps a strong MgO signal.
[c] Surface area.

other two important spinel signals, which should be observed at $2\theta = 43.13$ and 62.54° (relative intensities 26 and 47%, respectively), overlap the MgO ones. α-Fe_2O_3 is not detected by XRD in Fe/MgO, its main signal being absent ($2\theta = 33.16°$). Since the Fe/Mg ratio is higher for the model spinel compound than for the Fe(w)/MgO series, it is possible to detect the presence of α-Fe_2O_3 by XRD as segregated phase in the former, but not in the latter.

From these results we could conclude that catalysts are made up of spinel and MgO only. Let us see what Raman spectroscopy can show us about this system.

The Raman spectrum corresponding to α-Fe_2O_3 presents (Table 1) two very weak signals at 612 and 498 cm^{-1}. For $MgFe_2O_4$ three main Raman signals are detected at 714, 542, and 472 cm^{-1}, with a small shoulder at 638 cm^{-1} on the first one. The support, just like for the sample with a 1.5% Fe content, does not present Raman signals but does show fluorescence. The other catalysts of the Fe/MgO series clearly show the spinel fingerprint. The Fe(3)/MgO sample presents some fluorescence, on which the spinel signals are mounted. In the Fe(6)/MgO sample, the fluorescence has sharply decreased and completely disappeared in the Fe(9)/MgO sample. The absence of α-Fe_2O_3 bands in the Fe/Mg system does not preclude the presence of the iron oxide since its Raman spectrum is very weak. Note that the spectrum of the spinel model compound does not show the bands of α-Fe_2O_3 despite the fact that the oxide was clearly seen by XRD.

Mössbauer Spectroscopy

The Mössbauer parameters (hyperfine magnetic fields, isomer shifts, and quadrupole splitting) corresponding to the $MgFe_2O_4$ model sample at 298 K and at 16 K are in good agreement with the ones reported for the bulk spinel (14). The observed sextuplet spectrum (Fig. 1) can be fitted with three sextuplets, two of them assignable to Fe^{3+} located at tetrahedral and octahedral sites in the spinel structure while the third one has Mössbauer parameters coincident with those of α-Fe_2O_3 detected by XRD (Table 1). Considering the oxide parameters, it was estimated that the spinel phase contained ca. 20% segregated oxide.

In the spectra of the Fe/MgO catalysts at room temperature, the signal is composed of a doublet and a sextuplet in every case. Figure 1A shows the spectra corresponding to Fe(1.5)/MgO and Fe(9)/MgO as representative of the series. The sextuplet may be assigned ot the $MgFe_2O_4$ species. The doublet may be due either to α-Fe_2O_3 or to very small crystals of the spinel showing superparamagnetic relaxation, or paramagnetic isolated Fe^{3+} ions, dispersed in the MgO matrix. The spectra of the same catalysts at 16 K (Fig. 1B) confirm the existence of $MgFe_2O_4$ in the solid. If the central signal belongs to very small crystallites when the temperature is lowered, the doublet area should decrease with the increase of the sextuplet area. If the composition of these small crystallites were $MgFe_2O_4$, only two sextuplets would remain. On the other hand, if they were α-Fe_2O_3 crystals, a new one would appear. However, neither happens. Besides, the Mössbauer parameters of this central signal are almost identical for all the samples. Thus, everything indicates that this signal is due to Fe^{3+} ions dispersed in the MgO lattice. According to these results, the catalysts are made up of zones with $MgFe_2O_4$ structure and Fe^{3+} ions dispersed in the MgO matrix. The amount of spinel in the catalysts increases with higher iron loading, as shown in Table 2. The most reliable percentages of each species are those measured at low temperature, since under these conditions, the probable differences in the recoil free factors are minimal.

The moles of Fe^{3+} and $MgFe_2O_4$ per gram of catalyst were calculated by taking into account that the only detectable species in the catalysts are MgO, Fe^{3+} dispersed in the support matrix (whose ionic charge is balanced by oxide ions), and $MgFe_2O_4$. The quantification obtained by the Mössbauer spectroscopy (Table 2) was used. These calculations show that the amount of Fe^{3+} stays essentially

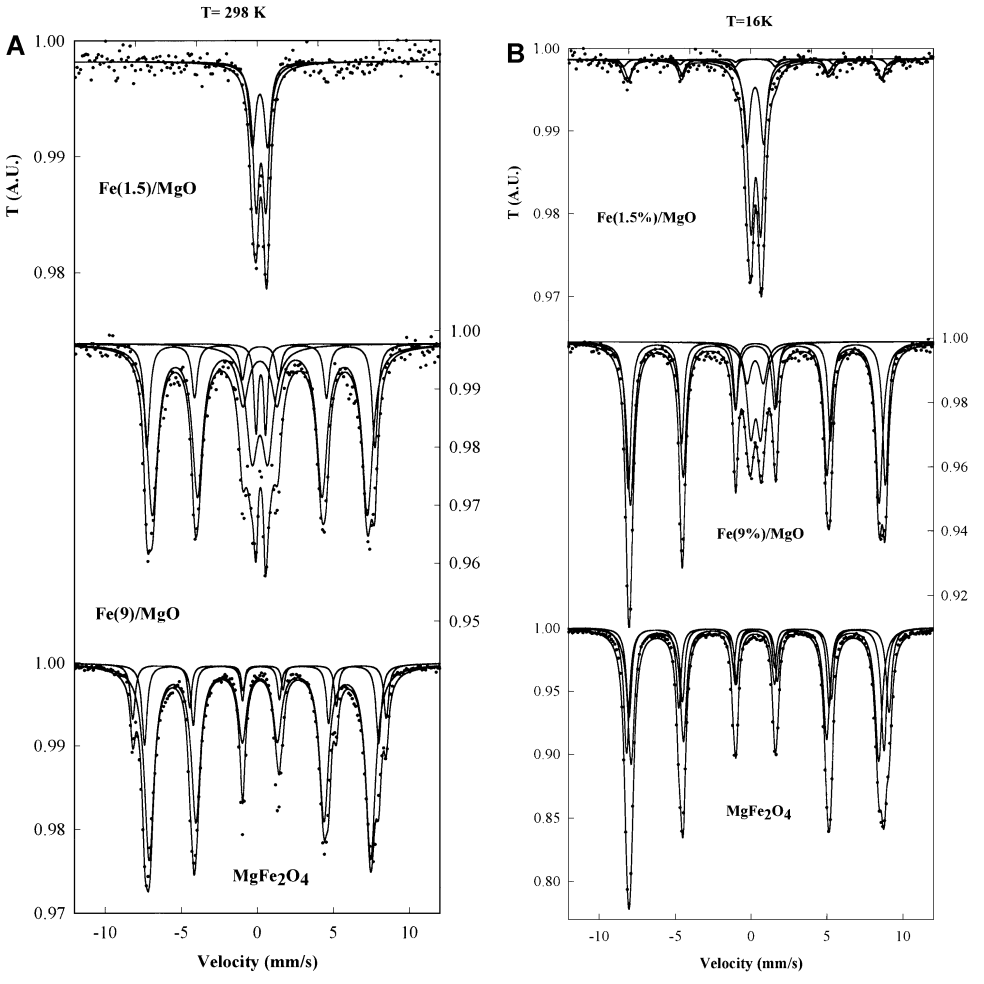

FIG. 1. Mössbauer spectra of Fe(1.5)/MgO, Fe(9)/MgO, and the model compound $MgFe_2O_4$, (A) at room temperature and (B) at 16 K.

constant while the spinel amount increases by a factor of 23 (Fig. 2). This seems to indicate that at low iron concentrations, finely dispersed Fe^{3+} ions are formed and as the iron load increases above ca. 1%, the spinel phase starts to develop. Therefore, it seems that a threshold concentration of iron must be reached to form the spinel in the MgO matrix.

TABLE 2

Atomic Percentage Corresponding to Iron as Spinel and as Fe^{3+} Calculated from the Mössbauer Spectra for Fe/MgO

		Catalyst			
T (K)	Species	Fe(1.5)/MgO	Fe(3)/MgO	Fe(6)/MgO	Fe(9)/MgO
298	$MgFe_2O_4$	—	51 ± 2	64 ± 3	77 ± 4
	Fe^{3+}	100	49 ± 1	36 ± 2	23 ± 2
16	$MgFe_2O_4$	18 ± 2	50 ± 5	65 ± 4	79 ± 5
	Fe^{3+}	82 ± 5	50 ± 2	35 ± 1	21 ± 1

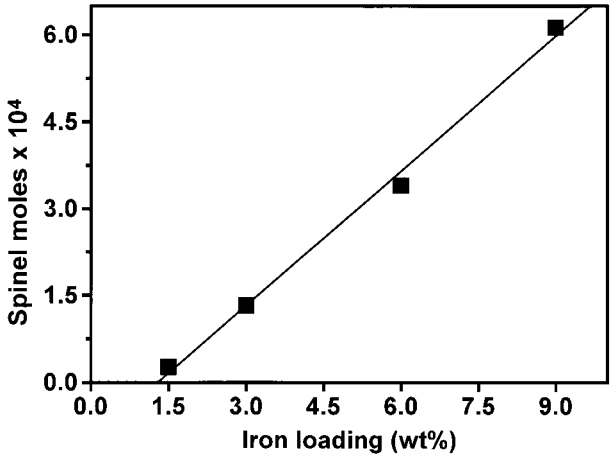

FIG. 2. Dependency of the amount of $MgFe_2O_4$ formed in the Fe/MgO catalysts on the iron loading. The moles indicated are referred to 1 g of catalyst.

Which iron-containing phase is the active one? This question will be addressed after reporting the catalytic data obtained.

Micrographs and EPMA

The micrographs of magnesia powder calcined at 1073 K (1,500 and 4,000 × magnification) are shown in Fig. 3A. It can be seen that the particles of the support present a "flake" structure. Some flake agglomerates on the top of the particles are also observed. These agglomerates are randomly distributed. Magnesia supported iron ($w = 3$, 6, and 9 wt%) shows the same "flake" structure and agglomerates as MgO, as seen in the micrograph of Fe(9)/MgO powder (Fig. 3B).

The electron probe microanalysis of Fe(9)/MgO reveals a significant heterogeneity in the composition of the particles (Table 3). The ratio of Mg/Fe increased when the volume analyzed was mainly formed by "flake" agglomerates, suggesting that the main component of these agglomerates is Mg. This effect was also observed in particles of Fe(6)/MgO.

TABLE 3

Semiquantitative Elemental Probe Microanalysis (EPMA) Results

Sample	Mg[a]	Fe[a]	Mg/Fe[b]
Fe(6)/MgO	89	11	11.21
	89	11	11.21
	85	15	7.85
Fe(9)/MgO	81	19	5.91
	78	22	4.91
	71	29	3.39
	80	20	5.54
$MgFe_2O_4$[c]	13	87	0.21

[a] Relative amounts in wt%.
[b] Atomic ratio.
[c] The $MgFe_2O_4$ stoichiometric compound has an Mg/Fe ratio of 0.5.

Catalytic Measurements

The raw kinetic data obtained at one fixed reactant concentration ($CH_4 = 2\%$ v/v, $O_2 = 8\%$ v/v, balance N_2) in the temperature range of 848–948 K is plotted in Fig. 4 versus the iron loading. These data show that the addition of iron

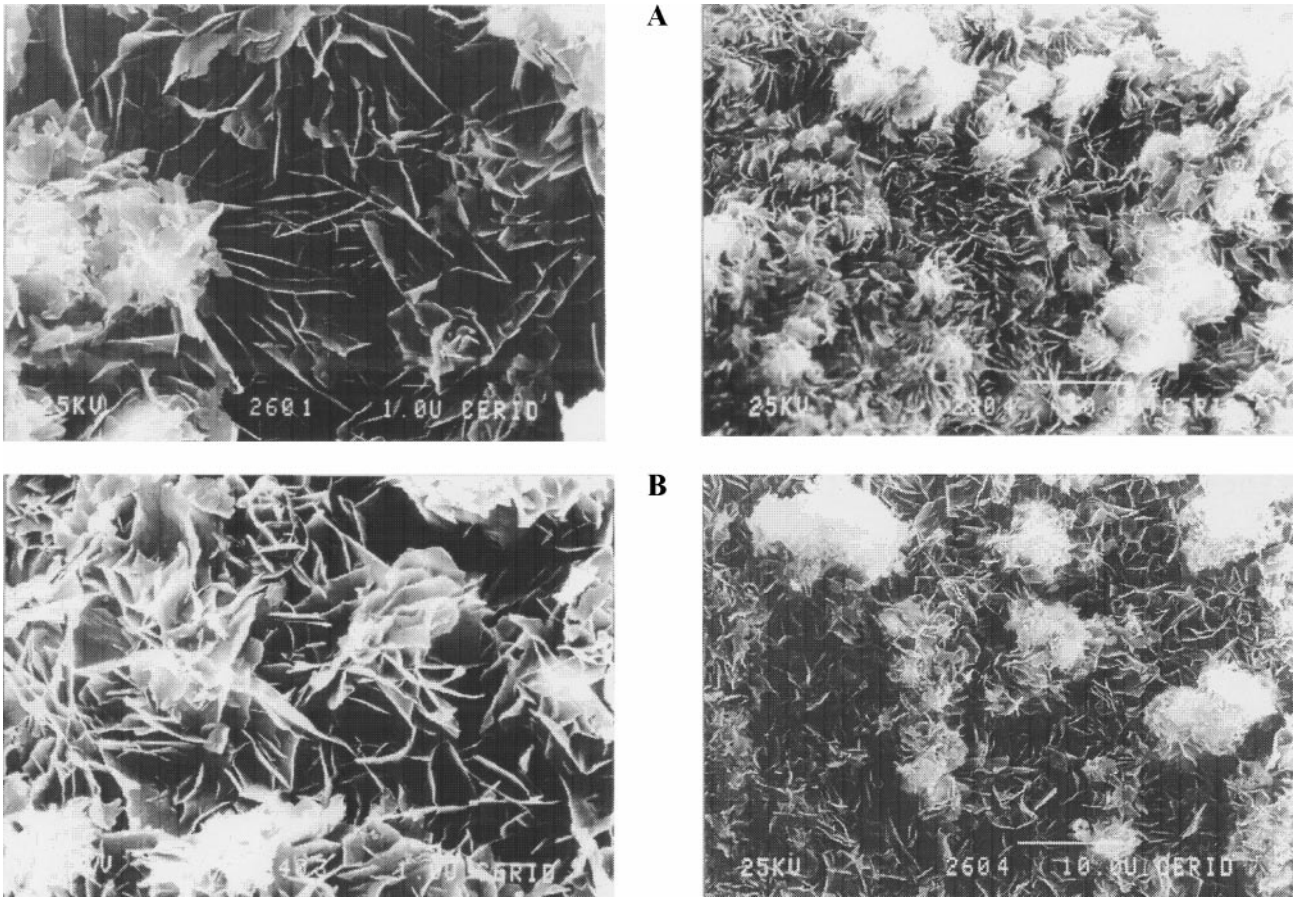

FIG. 3. Micrographs of (A) the support MgO and (B) Fe(9)/MgO, both with 1,500 and 4,000 × magnification.

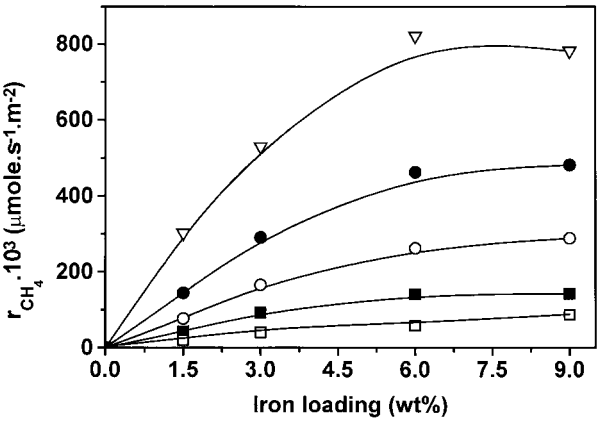

FIG. 4. Methane combustion rate as a function of the iron loading. Symbols: (□) 848 K, (■) 873 K, (○) 898 K, (●) 923 K, and (▽) 948 K. Feed: CH_4, 2% v/v, O_2, 8% v/v, balance N_2.

to MgO catalyzes the total methane oxidation, while the support itself is inactive under the reaction conditions here reported. As the iron loading increases, the catalytic activity is enhanced but a saturation value is achieved at every temperature when the iron content is 6% or more. Note that the specific surface area decreases monotonically with increasing iron content (Table 1).

The spinel was also catalytically tested in order to compare its activity with the one corresponding to the saturation value at the highest temperature (948 K). This experiment is hard to perform without uncertainty due to the low surface area of the spinel (Table 1). Thus, it was carried out employing 1.006 g of spinel and a space velocity of 63,500 h^{-1}. At 948 K, a reaction rate value of 0.9 $\mu mol \cdot s^{-1} \cdot m^{-2}$ was determined for the spinel, which differs by ca. 10% from the saturation value observed at this temperature (Fig. 4).

If the raw kinetic data were plotted versus the spinel concentration calculated from the Mössbauer spectra, the same trend would be obtained, as expected from the linear relationship between the concentration of this species and that of total Fe (Fig. 2). No correlation is obtained, however, if the same plot is made against the Fe^{3+} concentration. This seems to indicate that the active sites are located on the spinel phase.

Before further discussion, the possibility of mass transfer limitations should be checked. Hickman and Schmidt (15) worked at residence times between 10^{-4} and 10^{-2} seconds in their study on methane direct oxidation to explore synthesis gas generation, finding significant mass transfer effects. Although their conditions and catalytic configuration (Pt monolith, a very active catalyst, methane concentration higher than 16%) are quite different from ours, the contact times employed in our experiments were similar. In order to quantitatively check the importance of the pore diffusion limitations, the Weisz-Prater modulus can be applied: $\Phi = r_{CH_4} L^2 / D_{eCH_4} C_{CH_4}$. The parameters in this modulus were calculated assuming the most unfavorable conditions:

$$r_{CH_4} = 1.28 \times 10^{-9} \text{ mol} \cdot \text{s}^{-1} \text{ cm}^{-3} \ (x_{CH_4} = 12.9\%)$$
$$L = 4.2 \times 10^{-3} \text{ cm}$$
$$D_{e\,CH_4} = 1.503 \text{ cm}^2 \cdot \text{s}^{-1}$$
$$C_{CH_4} = 2.572 \times 10^{-7} \text{ mol} \cdot \text{cm}^{-3}$$
$$(\bar{p}_{CH_4} = 2\text{kPa}; T = 948.15 \text{ K}).$$

Replacing these data, $\Phi = 6 \times 10^{-8} \ll 1$. The same order of magnitude is obtained for O_2. If in the smaller pores one assumes a Knudsen regime, the Φ values are still very low. These calculations confirm the absence of mass transport limitations.

Another issue to be considered, given the combustion exothermicity, is the temperature gradient inside the catalyst particles. Combining the continuity and energy equations, and taking into account that the maximum conversion achieved was 12.9%, and particle size 60–80 mesh, we obtained $\Delta T = 12.7^\circ$C. For the average conversion value (5%) used in our rate calculations, this temperature increase went down to 4.9°C.

DISCUSSION

The diffraction patterns and particularly the Raman spectra clearly show the presence of the $MgFe_2O_4$ spinel in Fe/MgO. However, an overall picture of the solid structure and a quantification of the different iron species were obtained using Mössbauer spectroscopy. At low Fe content (ca. below 1 wt%) Fe^{3+} cations are finely dispersed in the MgO matrix while at higher metal concentrations the spinel phase develops. From about 1 wt% up to 9 wt% Fe, the spinel concentration increases linearly as shown in Fig. 2, while the Fe^{3+} concentration remains essentially constant.

This picture of the Fe/MgO system in the oxidized form is consistent with the findings of Boudart and co-workers (7–9) who studied this system but in its reduced form. They detected Fe^{2+} clusters in MgO and found that the concentration of these clusters only varied a little with the total iron loading, up to 40%. In agreement with our results, Fe cations seemingly tend to form a solid solution with the magnesium oxide before forming the main phase, having to overcome a threshold concentration. According to Boudart and co-workers (7–9) the phases present in the Fe/MgO catalysts in their reduced form are Fe^{2+} cations dispersed in MgO (FeO–MgO solid solution) and Fe°, while in the oxidized form, according to our results there would be Fe^{3+} cations dispersed in MgO and $MgFe_2O_4$.

Asakura and Iwasawa (13) studied the Fe(5%)/MgO system in its oxidized form. They found small clusters of $MgFe_2O_4$ in the MgO lattice and explained the high activity obtained with these catalysts by the combination of coordinately unsaturated basic O^{2-} sites and acidic Fe^{3+}

sites. According to these authors, these acidic Fe^{3+} would be cations with low coordination number, located at the interface between MgO and the $MgFe_2O_4$ clusters. However in our case, the catalytic behavior of the Fe/MgO system for methane combustion does not correlate with the Fe^{3+} concentration in the MgO matrix (*vide infra*). On the other hand, there is a nonlinear relationship between the reaction rate and the spinel concentration.

The most straightforward explanation for the catalytic behavior of the Fe/MgO series with iron concentration, namely the complete coverage of the catalyst surface with the active site, is supported by neither SEM micrographs (Fig. 3) nor EPM analyses (Table 3). They show that even the Fe(9)/MgO catalyst contains islands of MgO decorating the catalyst surface. These results reveal a noticeable surface heterogeneity in the Fe/MgO catalysts, being more important in the most concentrated sample (9%). This heterogeneity is expressed in an enrichment of Mg in different zones of the samples. The origin of the MgO islands and of this heterogeneity is discussed below.

Let us consider the different stages of the impregnation process. When MgO is in contact with water, the total conversion to hydroxide is thermodynamically favored. When the iron nitrate solution is mixed with the magnesium hydroxide suspension, the iron hydroxide precipitation occurs. Ferric ions in aqueous solution have a tendency to hydrolysis and/or complex formation. At pH higher than ca. 2, polynuclear species are formed, equilibrium is reached more slowly, and colloidal gels develop (16). The equilibrium system of the different complexes in aqueous solution was solved, for both iron and magnesium, after the suspension was mixed with the ferric solution (17). In every case (preparation of the whole series of catalysts), a pH of 9.3 was obtained while the calculated concentration of all the complexes was very small.

According to these results, during the impregnation process, when the ferric solution gets in contact with the magnesium hydroxide suspension, the total precipitation of the Fe^{3+} cation takes place. At the same time, in order to satisfy the electroneutrality in solution (presence of the nitrate anions) an equivalent amount of Mg^{2+} is solubilized. Ferric hydroxide precipitates on $Mg(OH)_2$ in the form of a slow nucleation gel. During the drying process, a final deposition of $Mg(NO_3)_2$ on the solid takes place. In the calcination stage, the former becomes MgO, covering the impregnated Fe, thus forming islands on the catalyst surface.

The shape of the activity curves (Fig. 4) can now be rationalized. In view of the above analysis when the Fe loading increases, the amount of reprecipitated MgO also goes up. These two factors have opposite effects on the catalytic activity and may lead to the plateaus observed in these plots. The crystallite size values for both species estimated from the XRD data agree with this reasoning. For $MgFe_2O_4$ in Fe/Mg, the crystallite size increases from 267 to 344 Å (samples with 3, 6, and 9% iron; in the 1.5% sample the spinel phase is not detected by XRD), whereas for the bulk spinel it is 473 Å. For MgO this increase is also observed, ranging from 298 to 409 Å. In brief, from an iron loading of 6% and higher the increase in the amount of impregnated iron does not improve the activity due to the reprecipitation of MgO on the catalyst surface.

The reaction rate equation may be written as

$$r = kF(T, \bar{p}_{O_2}, \bar{p}_{CH_4}),$$

where k is the surface reaction rate constant. This magnitude is a function of the amount of active sites (w) through the preexponential factor (A) of the Arrhenius equation:

$$r = A(w)\exp\left(\frac{-E_a}{RT}\right)F(T, \bar{p}_{O_2}, \bar{p}_{CH_4})$$

When the plateau is reached (Fig. 4) at each temperature, the following results:

$$r_{max} = A(w_{max})\exp\left(\frac{-E_a}{RT}\right)F(T, \bar{p}_{O_2}, \bar{p}_{CH_4})$$

At constant temperature and partial pressure of the reactants the ratio r/r_{max} reflects the behavior of A/A_{max}. Figure 5 shows that this ratio correlates with the amount of spinel measured in each catalyst sample. No correlation was found, however, when the amount of Fe^{3+} was plotted in the abscissa. Therefore, Fig. 5 is consistent with the role played by the spinel phase as loci of the active sites for methane combustion.

The MgO is necessary only to provide enough specific surface (which the spinel alone cannot develop) and to form the spinel, but it would not participate in the reaction. In favor of this statement we have the result of the measurement of the spinel catalytic activity.

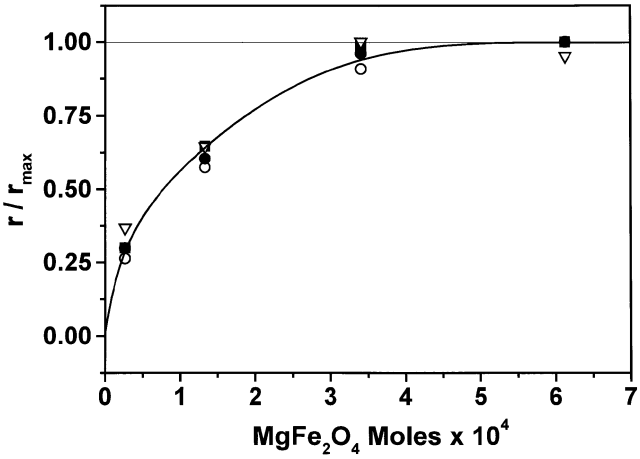

FIG. 5. Evolution of the methane combustion rate referred to the maximum at each temperature as a function of the spinel amount per gram of catalyst. Symbols: (■) 873 K, (○) 898 K, (●) 923 K, and (▽) 948 K.

CONCLUSIONS

- Fe/MgO calcined at 1073 K is made up of $MgFe_2O_4$ crystallites that develop when the iron loading is higher than ca. 1 wt%. They coexist with Fe^{3+} cations dispersed in the MgO matrix.
- Between 1.5 and 9 wt% iron loading, the Fe^{3+} weight fraction remains almost constant while the spinel concentration increases by a factor of 23.
- The methane combustion rate increases with the spinel weight fraction but reaches a plateau at ca. 6 wt% Fe loading (Fig. 4). This is due to the partial solubilization of Mg^{2+} which reprecipitates upon drying, decorating the catalyst surface (Fig. 3 and Table 3).
- All the experimental data reported here favor the hypothesis that the active sites are located on the spinel phase.

ACKNOWLEDGMENTS

The authors acknowledge the financial support received from CONICET, ANPCyT, and UNL (CAI+D '96). Thanks are also given to the Japan International Cooperation Agency (JICA) for the donation of the XRD and Raman instruments, and to Elsa Grimaldi for her help in the English edition of the manuscript.

REFERENCES

1. Pfefferle, L. D., and Pfefferle, W. C., *Catal. Rev.* **2**, 219 (1987).
2. XONON Systems, catalytica-inc.com, October 8, 1998.
3. Arai, H., and Fukuzawa, H., *Catal. Today* **26**, 217 (1995).
4. Zwinkels, M. F. M., Järås, S. G., and Menon, P. B., *Catal. Rev. Sci. Eng.* **35**, 319 (1993).
5. Trimm, D. L., *Catal. Today* **26**, 231 (1995).
6. Berg, M., and Järås, S. G., *Appl. Catal. A: General* **114**, 227 (1994).
7. Boudart, M., Delbouille, A., Dumesic, J. A., Khammouna, S., and Topsøe, H., *J. Catal.* **37**, 486 (1975).
8. Dumesic, J. A., Topsøe, H., Khammouma, S., and Boudart, M., *J. Catal.* **37**, 503 (1975).
9. Dumesic, J. A., Topsøe, H., and Boudart, M., *J. Catal.* **37**, 513 (1975).
10. Ueda, W., Yokoyama, T., Moro-Oka, Y., and Ikawa, T., *J. Chem. Soc., Chem. Commun.* **391** (1984).
11. Ueda, W., Yokoyama, T., Moro-Oka, Y., and Ikawa, T., *Ind. Eng. Chem. Prod., Res. Dev.* **24**, 340 (1985).
12. Ueda, W., Kurokawa, H., Moro-Oka, Y., and Ikawa, T., *Chem. Lett.* **39** (1985).
13. Asakura, K., and Iwasawa, Y., *Mater. Chem. Phys.* **18**, 499 (1988).
14. De Grave, E., Govaert, A., Chambaere, D., and Robbrecht, G., *Physica B* **96**, 103 (1979).
15. Hickman, D. A., and Schmidt, L. D., *J. Catal.* **138**, 267 (1992).
16. Cotton, F. A., and Wilkinson, G., "Advanced Inorganic Chemistry," 2nd Ed., Interscience, New York, 1967.
17. Spretz, R., Ph. D. Thesis, Universidad Nacional del Litoral, Argentina, 1998.